Research Article

Reem M. Alghanmi*, Ragaa A. Hamouda, Aisha H. Al-Moubaraki, Afnan A. Allouzi, and Muhammad A. Abuelmagd

Biofabrication of silver nanoparticles using *Uncaria tomentosa* L.: Insight into characterization, antibacterial activities combined with antibiotics, and effect on *Triticum aestivum* germination

https://doi.org/10.1515/gps-2023-0207
received October 15, 2023; accepted January 15, 2024

Abstract: Herein, we used the aqueous extract of *Uncaria tomentosa* L. barks (Cat's claw bark [CCb]) for the biofabrication of silver nanoparticles (CCb-Ag-NPs). The effects of different parameters (*Uncaria tomentosa* L. aqueous extract, silver nitrate [$AgNO_3$] ratio, temperature, and pH) on the formation of the nanoparticles were investigated using UV scan as a preliminary tool for the detection of surface plasmon resonance of CCb-Ag-NPs. The optimal ratio was 1:7 (*Uncaria tomentosa* L. extract: 1 mM $AgNO_3$ solution). Fourier-transform infrared spectroscopy revealed the functional groups of both CCb extract and the CCb-Ag-NPs, whose dispersion and quasispherical morphologies were characterized using scanning electron microscopy and transmission electron microscopy. Particle sizes ranged from 19.2 to 38.5 nm. The zeta potential of CCb-Ag-NPs was −34.44 mV. According to energy-dispersive X-ray analysis, the CCb-Ag-NPs contained 28.87% silver. The formation of Ag-NPs was also confirmed by X-ray diffraction pattern analysis. Pristine CCb-Ag-NPs showed antibacterial activity against three pathogenic bacterial strains: *Escherichia coli* (ATCC 25922), *E. coli* (ATCC 8739), and *Pseudomonas aeruginosa* (ATCC 90274). Antibacterial activity increased significantly after loading CCb-Ag-NPs on antibiotic discs containing meropenem and cefoxitin. Low concentrations of CCb-Ag-NPs also enhanced the germination percentage, coleoptile length, and radical root length of *Triticum aestivum*.

Keywords: silver nanoparticles, *Uncaria tomentosa* L., antibacterial activity, hemolysis activity, wheat germination

1 Introduction

A major global concern regarding the use of most antibiotics is the growing resistance of bacteria to these antibiotics, which has led to substantial health consequences in recent decades [1]. Microorganism resistance, which was initially characterized by the development of treatment resistance in microorganisms, lowered therapeutic indices, toxicity, side effects, non-specific effects, and dosage issues, has been caused by the frequent use of antibiotics [2]. Better-acting antibiotics have been sought after continually during the resistance period, alongside the increase in antibiotic resistance over the past 10 years, mostly due to the common and improper use of these therapeutic medicines [3]. Silver nanoparticles (Ag-NPs) have emerged as one of the most promising materials for combating drug-resistant bacteria due to their remarkable antibacterial characteristics. In that case, nanoscience and nanotechnology are focused on the synthesis, characterization, and applications of nanostructured materials. These materials have at least one dimension that is in the nanoscale range. The ability to pattern and describe materials at the nanoscale is driving a revolution in materials science and

* **Corresponding author: Reem M. Alghanmi,** Department of Chemistry, College of Science, University of Jeddah, Jeddah 21589, Saudi Arabia, e-mail: rmalghanmi@uj.edu.sa
Ragaa A. Hamouda: Department of Biology, College of Sciences and Arts Khulais, University of Jeddah, Jeddah, Saudi Arabia; Genetic Engineering and Biotechnology Research Institute, University of Sadat City, Sadat City, Egypt
Aisha H. Al-Moubaraki, Afnan A. Allouzi: Department of Chemistry, College of Science, University of Jeddah, Jeddah 21589, Saudi Arabia
Muhammad A. Abuelmagd: Department of Botany, Faculty of Science, Mansoura University, Mansoura, Egypt; Faculty of Pharmacy, Mansoura National, Egypt University, Gamasa 7731168, Egypt

engineering. Comparing similar materials in the bulk and nanoscales might show remarkably contradictory characteristics. The primary reason for these different properties of nanoparticles, aside from the underlying and physicochemical properties of the metals in issue, is the extreme shift in surface-to-volume ratios as we enter into the nanoscale [4,5]. Nowadays, nanoscience contributes to the production of a wide range of various synthesized metal nanoparticles (MNPs). Also, MNPs have exceptional electrical, optical, magnetic, and mechanical characteristics and are being created at a rapid pace for applications in bioengineering, information technology, energy, and the environment, as well as usage in drug delivery and bioimaging [6]. A major factor in the development of advanced nanomedicines is the successful application of various nanoparticle- and nanotechnology-based therapies against pathogenic microorganisms [7].

The noble metal silver is inert and relatively stable compared to other metals and has a highly positive electrochemical potential (0.80 V); thus, it has been interesting recently because it is well-suited for the fabrication of nanoparticles [8–10]. Notably, the slow leaching of Ag^+ ions is harmful to pathogens but not normal cells [11–13]. Ag-NPs have a wide spectrum of bactericidal and fungicidal activities as well as the ability to coordinate with various ligands and macromolecules in microbial cells. Also, Ag-NPs have been widely used in the control of microbial proliferation as well as in curing wound healing due to their anti-inflammatory effects. Due to their antioxidant properties, Ag-NPs are extremely useful in the prevention and treatment of diseases [3,4,14]. As an alternative to "nanoscale antibiotics," the term "nanobiotics" was recently introduced in medical science. It was reported that Ag-NPs have been used in conjunction with certain antibiotics, and these AgNPs have been demonstrated to kill around 650 disease-causing microorganisms without endangering human health [7]. This combination has made it possible to resolve several problems related to antibiotic-resistant microorganisms.

Ag-NPs can be fabricated physically and chemically using different techniques. Physical techniques involve elaborate procedures that have the disadvantage of a lack of size control. Chemical techniques used are sol–gel, chemical co-precipitation, and electrochemical and hydrothermal methods. These techniques have some disadvantages, such as requiring organic solvents and harsh conditions in addition to being expensive and having hazardous effects on the environment. However, the use of green synthesis techniques provides cost-effective, simple, and safe fabricated techniques. Additionally, they make use of renewable resources and non-toxic chemicals, which finally leads to a decrease in waste and pollution [15]. In the fabrication of Ag-NPs, green synthesis strategies use naturally biodegradable components, such as polysaccharides, biopolymers, vitamins, plant extracts, and microorganisms, microbial enzymes, fungi, and extract of different parts from plants [16,17]. Due to their reducing properties, such extracts can help incorporate silver ions into nanoparticles. Plant-derived biomolecules like tannins, alkaloids, and terpenoids are easy to handle and maintain while serving as reducing, capping, and stabilizing agents [18]. Recently, plant extracts from several species, such as seeds [19], leaves [20–22], fruits [23], bark [24,25], woodchips [26], and roots [5,27], have been investigated for their ability to generate metallic nanoparticles. However, the optimal conditions for plant-based nanoparticle synthesis remain unclear [5,28]. Ag-NPs can benefit from low toxicity and biocompatibility of plant-based synthesis that enables widespread use. Water is primarily employed as the extraction solvent when employing plant extracts to create Ag-NPs. In some cases, an ethanol or methanol solution was also used [29]. Cat's claw is a popular name for the medicinal plant *Uncaria tomentosa* L., whose thorns resemble claws [30]. Cat's claw bark (CCb) is rich in alkaloids, polyphenolics, including hydroxybenzoic acid and tannins, and flavonoids [31]. Many diseases can be treated with the inner bark of this plant, like rheumatoid arthritis, diabetes, and allergies. The anti-inflammatory and polyphenolic compounds extracted from this inner bark can also be used to prevent some cancers [32,33].

To the best of our knowledge, no studies have been published on the biological applications of nanoparticles fabricated using the CCb extract. Thus, this study focuses on the applications of Ag-NPs that are fabricated using an aqueous extract of *Uncaria tomentosa* L. as a reducing and stabilizing agent. The surface plasmon resonance (SPR) absorption spectra of the CCb extract and fabricated CCb-Ag-NPs under different conditions were assessed by UV–Vis spectrophotometry. The functional groups of the CCb aqueous extract and the fabricated CCb-Ag-NPs were identified using Fourier-transform infrared spectroscopy (FT-IR). The physicochemical properties such as size, shape, size distribution, and X-ray diffraction (XRD)-based composition were analyzed using scanning electron microscopy (SEM), transmission electron microscopy (TEM), XRD, energy-dispersive X-ray spectroscopy (EDS), and zeta potential analysis techniques. The important aim of this study was to investigate the antibacterial activity of meropenem/loaded CCb-Ag-NPs (MEM/CCb-Ag-NPs) and cefoxitin/loaded CCb-Ag-NPs (FOX/CCb-Ag-NPs) against three pathogenic bacterial strains: *Escherichia coli* (ATCC 25922), *E. coli* (ATCC 8739), and *Pseudomonas aeruginosa* (ATCC 90274). Additionally, the effect of CCb-Ag-NPs on wheat seed germination was studied. Finally, the hemolytic activity of the fabricated CCb-Ag-NPs was measured and evaluated.

2 Materials and methods

2.1 Materials

CCb was collected from Amman, Jordan. Silver nitrate ($AgNO_3$) was purchased from Sigma-Aldrich. All aqueous solutions were prepared using double-distilled water. All reagents used were of analytical grade.

2.2 Preparation of the CCb extract

CCb was washed several times with tap water and then twice with distilled water to remove the surface impurities. It was then dried for several days at room temperature. An automatic mortar was used to grind the bark into a homogenous fine powder. The powdered CCb was sieved using a sieve of size 250 µm. The aqueous extract of CCb was prepared by mixing 5.0 g of the finely ground CCb powder with 100 mL of distilled water at 4°C for 24 h with gentle shaking. Then, the aqueous extract was separated from the residue by centrifugation at 6,000 rpm for 20 min to obtain a clear solution, which was frozen until used for the biofabrication process (Figure 1).

2.3 Biofabrication of CCb-Ag-NPs

Ag-NPs were fabricated using the bottom-up method, as described by Zargar et al. [33], with some modifications. About 35.0 mL of 1.0 mM $AgNO_3$ solution was added to 5.0 mL of the CCb extract solution (5%). The mixtures were stirred for 30 min at 80°C using a hot plate stirrer. The color of the reaction mixture changed to brown and gradually became darker after 24 h of storage in dark bottles, which indicated the formation of Ag-NPs. The biofabricated Ag-NPs were separated by centrifugation at 10,000 rpm for 20 min and washed twice with distilled water to remove any organic contaminants. Ag-NPs were then lyophilized using a freeze-dryer (LABCONCO, Kansas, USA). Thus, the biofabricated AgNPs were ready for characterization and further study applications (Figure 2). The effective mixture ratio was investigated by adding different volumes of 1 mM $AgNO_3$ to 5 mL of the CCb extract to obtain a series of ratios (1:1, 1:3, 1:5, 1:7, and 1:9) (CCb extract:$AgNO_3$ solution). The optimal temperature for the biofabrication of CCb-Ag-NPs was determined by incubating the reaction mixture at 20, 40, 60, and 80°C. The optimal reaction time was investigated by incubating the reaction mixture at 80°C for 15, 45, 60, 120, 180, and 210 min. The impact of pH on the stability of the formed CCb-Ag-NPs was investigated by adjusting the pH of the reaction mixture to pH levels 5.6, 7, 8, and 9 using 0.1 M NaOH/HCl solutions.

2.4 UV–visible spectra of CCb-Ag-NPs

The SPR absorption spectra of the CCb extract and biofabricated CCb-Ag-NPs under different conditions were obtained in the scan range of 200–800 nm using a UV–visible spectrophotometer (Shimadzu UV-1800, Japan) with a 1.0 cm quartz cell.

2.5 Characterization of CCb-Ag-NPs

The functional groups of both the CCb aqueous extract and the biofabricated CCb-Ag-NPs were identified using FT-IR (Frontier FT-IR spectrometer, Perkin-Elmer, USA) from 4,000 to 400 cm^{-1}. The morphology of the biofabricated CCb-Ag-NPs was assessed by SEM operating at 30 kV (SEM, JEOL JSM-6510/v, Tokyo, Japan). The morphology and size of the particles of the biofabricated CCb-Ag-NPs were determined by TEM (JEOL JSM-6510/v, Tokyo, Japan) at the nanoscale. The XRD pattern of CCb-Ag-NPs was assessed with an X-ray diffractometer (PAN Analytical X-Pert PRO). The size of nanoparticles (D) was calculated according to Scherrer's equation:

Figure 1: CCb and its powder.

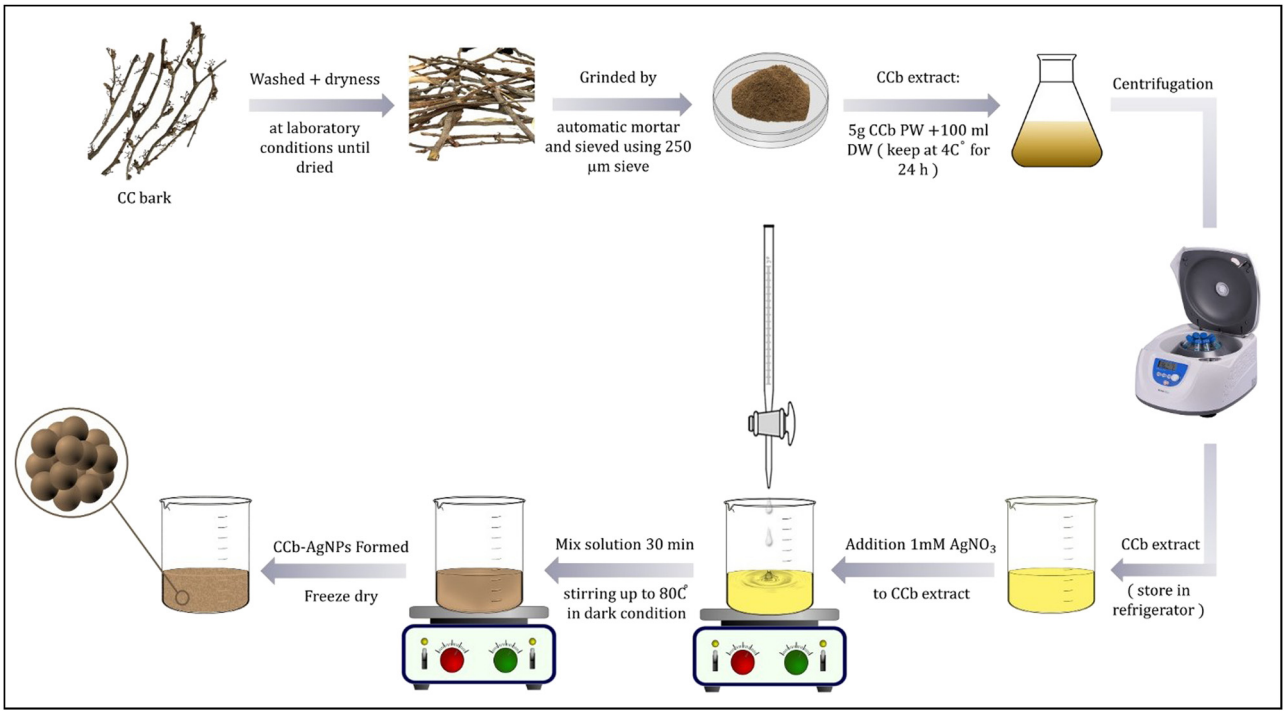

Figure 2: Schematic illustration of the biofabrication of CCb-Ag-NPs.

$$\text{Crystal size}(D) = \lambda k/\beta \cos\theta \quad (1)$$

where λ is the wavelength (nm) of the X-ray, β is the full width at half-maximum, and k is a constant related to the crystallite shape (=0.9). The value of β in 2θ axis of the diffraction profile is in radians.

A field emission scanning electron microscope equipped with EDS (JEOL JSM-6510/v, Tokyo, Japan) was used to examine the shape of the CCb-Ag-NPs. The zeta potential of the biofabricated CCb-Ag-NPs supports the aspects of stabilization in the middle of the liquid when it is dispersed (Malvern Zeta size Nano-Zs90, Malvern, USA).

2.6 *In vitro* biological activities

2.6.1 Antibacterial activities

The disk-diffusion method was used to assess the antimicrobial activity of pristine CCb-Ag-NPs, MEM/CCb-Ag-NPs, and FOX/CCb-Ag-NPs against three pathogenic bacterial strains *E. coli* (ATCC 25922), *E. coli* (ATCC 8739), and *P. aeruginosa* (ATCC 90274). Inhibition zones around the disks were measured according to Wikler as an ordinary scale for bacterial growth inhibition [34]. Three tested bacterial strains were incubated at 37°C for 48 h until the colony-forming units (CFUs) reached approximately 10^8 CFU·mL^{-1} in Luria–Bertani broth media. Pure cultures of bacterial strains (100 µL) were subcultured onto a Mueller Hinton Agar plate. A filter paper (Whatman No. 3) disc with a 6 mm diameter was saturated with 50 µL of the test solution (CCb-Ag-NPs, MEM/CCb-Ag-NPs, and FOX/CCb-Ag-NPs) and transferred to the sub-cultured bacteria. Pure meropenem and cefoxitin discs (10 mg·mL^{-1}) were used as controls, and plates were incubated at 37°C for 48 h.

2.6.2 Effect of CCb-Ag-NPs on wheat growth

Wheat seed germination was assessed as previously described [35,36] with some modifications. *Triticum aestivum* L. seeds were sterilized using 75% ethanol for 5 min, followed by washing with distilled water. The experiment was conducted using three replicates, and each group contained 40 seeds. Different concentrations of CCb-Ag-NPs were prepared at 10, 20, 40, 80, and 160 mg·mL^{-1}. Seeds were soaked for 8 h at the previously mentioned concentrations of CCb-Ag-NPs, and another group was soaked in distilled water as a control. The seed germination rate was estimated after 48 and 96 h. The soaked *Triticum aestivum* seeds were transferred into Petri dishes containing three sheets of filter paper, and an appropriate amount of water was added every day. The incubation conditions were 20 ± 2°C, a photocycle consisting of 12 h/12 h day/night, and

relative humidity of 65%. Seedling growth rates, the coleoptile length (CL), and radical root length (RRL) were estimated after 4 and 8 days.

2.6.3 Effect of CCb-Ag-NPs on erythrocyte hemolysis

The hemolytic activity of the fabricated CCb-Ag-NPs was measured using blood-contacting medical devices. Here, the *n* hemolytic effect of CCb-Ag-NPs was studied in the whole blood of two healthy male donors, where the hematocrit percentage was quantified as 42.6 ± 0.11% and 44.2 ± 0.18% and stabilized using potassium EDTA (10%) as an anticoagulant in a volume ratio of 10 µL EDTA to 1 mL blood. RBCs were washed three times using saline solution, and 100 µL of washed RBCs were incubated for 2 h at 37°C with 100 µL of different concentrations of CCb-Ag-NPs (5, 10, 20, 40, and 80 mg·mL^{-1}). Blank samples were prepared using distilled water as a positive control (complete hemolytic action) and saline as a negative control (no hemolytic action). Incubated samples were centrifuged for 5 min at 2,000 rpm. The percentage of RBC hemolysis triggered by direct contact between CCb-Ag-NPs and RBCs was detected by measuring the absorbance of the supernatant at 541 nm. Hemolytic activity was calculated using the following formula:

$$\text{Hemolysis} = \frac{(\text{AS} - \text{AP})}{(\text{AW} - \text{AP})} \times 100 \quad (2)$$

where AS is the absorbance of the sample, AP is the absorbance of PBS (negative control), and AW is the absorbance of distilled water (positive control).

2.6.4 Statistical analysis

The mean of determinations done in triplicate is the total of all values, according to the latest release of SPSS 16. The study employed a one-way analysis of variance to statistically analyze the data. The least significant difference is determined at the P 0.05 level.

3 Results and discussion

3.1 UV–Vis spectroscopy assessment of CCb-Ag-NPs

Cat's claw includes numerous powerful compounds, and the water-soluble mixtures present in the aqueous extract reliably stabilized the Ag-NPs and reduced metal ions. UV–Vis spectroscopy validated the creation and stability of Ag-NPs, whose dark brown color was due to the excitation of SPR and related to the size and intensity of CCb-Ag-NPs [37]. Figure 3 shows the stability of CCb-Ag-NPs at

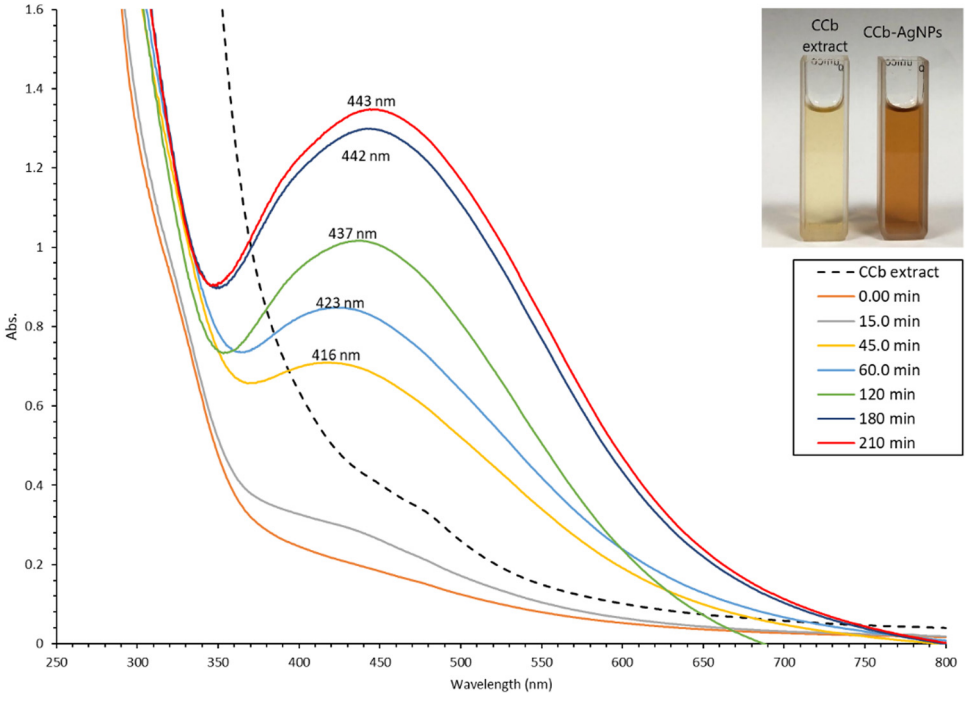

Figure 3: UV–Vis spectra of the CCb aqueous extract and CCb-Ag-NPs after 0, 15, 45, 60, 120, 180, and 210 min.

different time intervals from 0 to 210 min. The UV–Vis spectra reveal CCb-Ag-NP SPR bands centered at 416, 423, 437, 442, and 443 nm at intervals of 0, 15, 45, 60, and 120 min, respectively, and the stability of the CCb-Ag-NPs aqueous solution increased after 180 and 210 min. Intense bands were observed at 443 and 442 nm with absorbance intensities at 1.347 and 1.298, followed by broad bands at 437, 423, and 416 nm. It was reported that the UV–Vis spectra of Ag-NPs biofabricated with the *Mimusops elengi* L. leaf extract at 10, 30, 90, and 120 min, or 30 days were recorded at 434 nm [38]. Abo-Elmagd et al. [39] reported the highest absorption bands of the *Oscillatoria gelatin*-capped Ag-NPs that slightly shifted from 446 to 449 nm with increasing intensity of 0.8–1.6 by increasing the reaction time, and therefore, the NP size increased with increasing reaction time. The size, shape, and number of biofabricated Ag-NPs depend on the duration of exposure to silver ions [40]. A broad SPR band reflects the size of NPs, whereas broadband denotes the large size of NPs [41,42].

Different mechanisms for the green fabrication of metal NPs have been suggested by researchers. The possible mechanism for the fabrication of Ag-NPs in this study is illustrated in Scheme 1. The CCb aqueous extract contains organic phytoconstituents such as alkaloids, polyphenolics, tannins, and flavonoids, which react as biological reductants [31]. Silver ions in the salt solution accept electrons from the functional groups and reduce to silver zerovalent toms [4,6].

3.2 Effect of ratio, temperature, and pH on the biofabrication of CCb-Ag-NPs

Ag-NPs were fabricated with the CCb extract using different ratios, and 1:5 and 1:7 ratios of CCb aqueous extract to 1 mM $AgNO_3$ solution generated the highest SPR (Figure 4a). The 1:7 ratio was optimal for further experiments because its band was centered at a shorter wavelength compared with that of the 1:5 ratio. Previous work [43] showed that the size of the nanoparticles decreased, so the SPR shifted to shorter wavelengths. The optimal heating temperature for the biofabrication of Ag-NPs using the CCb extract was determined by UV–Vis spectroscopy. Figure 4b shows the increase in the SPR of Ag-NPs when the temperature of the mixture was raised from 20°C to 80°C for 90 min. The highest intensity was observed at 80°C, which indicates that the rate of fabrication at room temperature can be increased by increasing the temperature of the mixture. Anees Ahmad et al. [44] showed that the absorbance of Ag-NPs synthesized using the *Euphorbia serpens* Kunth extract increased when the temperature increased from 30°C to 60°C, though the particles became polydispersed at high temperatures. The pH of the reaction largely determines the efficiency of the reaction. Figure 4c shows the SPR of the mixture of the CCb extract and silver salt incubated at 80°C for 90 min at various pH levels (5.6, 7.0, 8.0, and 9.0). pH 9.0 maximized the fabrication of Ag-NPs with an absorption band centered at 412 nm. However, at pH 5.6, a broad band centered at 439.5 nm

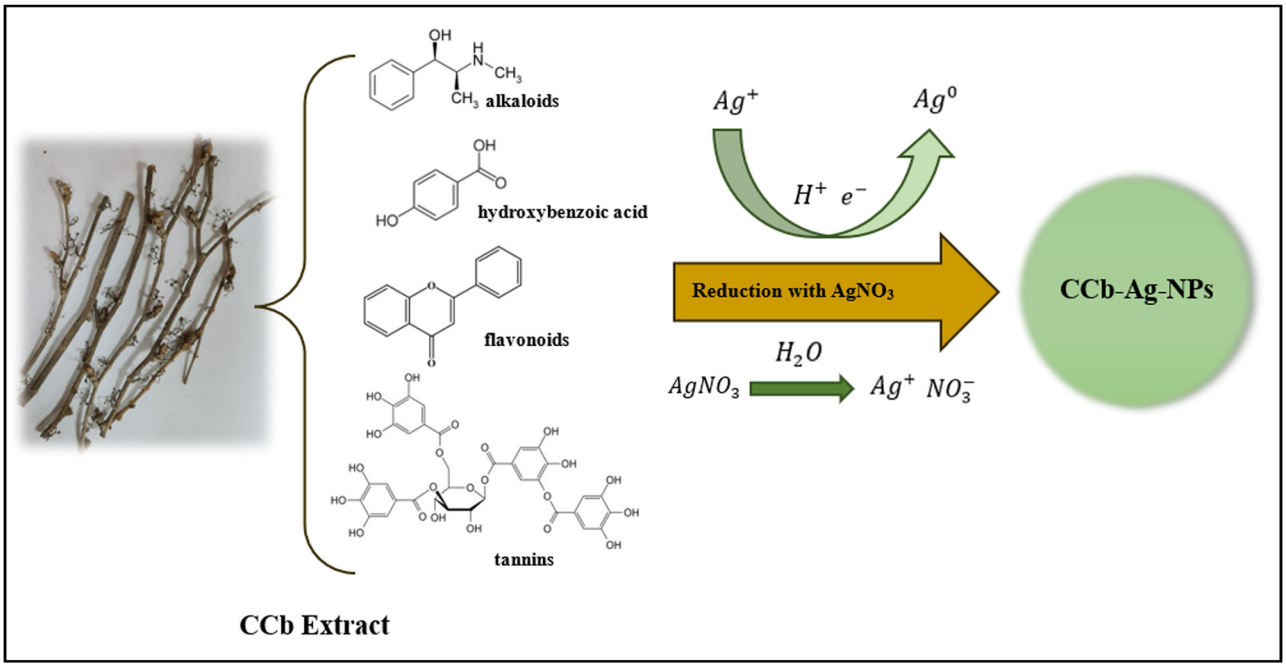

Scheme 1: Possible mechanism for the formation of CCb-Ag-NPs.

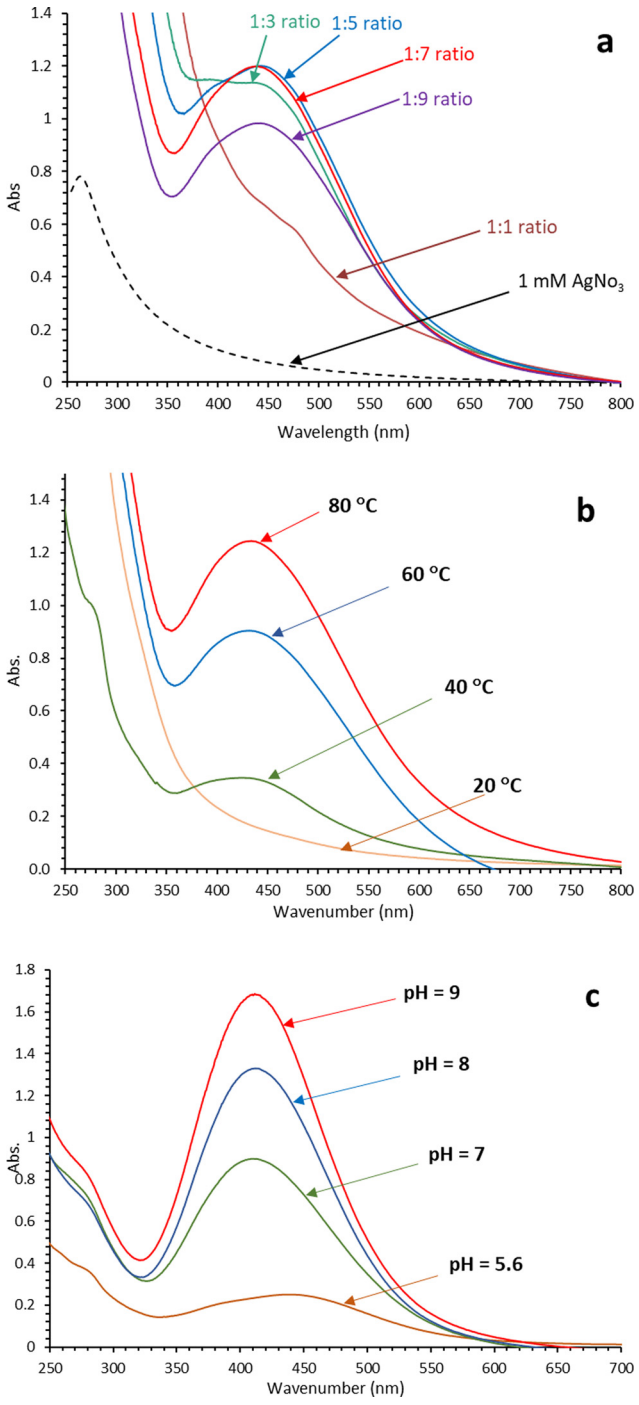

Figure 4: UV–Vis spectra of the biofabrication of CCb-Ag-NPs at different parameters: reactant mixture (CCb extract: $AgNO_3$) (a), temperature (b), and pH (c).

indicates the nonuniform particle size. Veerasamy et al. [45] claimed that more functional groups are available to bind silver under basic conditions, increasing the fabrication of Ag-NPs with smaller diameters. Other studies [25,46] also found that alkaline pH conditions are favorable for the fabrication of Ag-NPs.

3.3 Characterization of the biofabricated CCb-Ag-NPs

3.3.1 FT-IR assessment of CCb-Ag-NPs

Table 1 and Figure 5 show the FT-IR spectra of both CCb and CCb-Ag-NPs. CCb and CCb-Ag-NPs generated 11 and 10 peaks, respectively. The broad peaks at 3,421, 2,858, 1,742, 1,618, 1,446, 1,052, and 524 cm^{-1} in the CCb extract spectrum shifted to 3,414, 2,854, 1,729, 1,618, 1,446, 1,063, and 519 cm^{-1} in the CCb-Ag-NP spectrum, respectively. Three peaks in the FT-IR spectrum of the CCb extract at 1,319, 1,263, and 835 cm^{-1} were absent in the CCb-Ag-NP spectrum, whereas two peaks in the CCb-Ag-NP spectrum at 1,377 and 722 cm^{-1} were absent in that of the CCb extract spectrum. A band at 2,924 cm^{-1} was found in both spectra and was attributed to the asymmetric stretching vibrations of CH and CH_2. Overall, some peaks shifted to higher-frequency positions and others to lower-frequency positions; the active groups assigned to these peaks reduced the Ag ions and stabilized the CCb-Ag-NPs [47].

3.3.2 TEM and SEM analysis

The shapes and sizes of the biofabricated CCb-Ag-NPs were distinguished using SEM and TEM. CCb-Ag-NPs were well dispersed and quasispherical with anisotropic nanostructures (Figure 6), and their sizes ranged from 19.2 to 38.5 nm and showed a good distribution with no clusters. TEM has been

Table 1: Assignment of the FT-IR spectra of the CCb extract and CCb-Ag-NPs

CCb extract	CCb-Ag-NPs	Shift	Vibrational type	Reference
3,421	3,414	−7	Stretching vibration of the O–H bonds	[48]
2,924	2,924	–	Asymmetric stretching vibrations of CH_2	[49]
2,858	2,854	−4	CH_2 in the aliphatic compound	[50]
1,742	1,729	−13	ν(C═O)	[51]
1,618	1,624	+6	Amide I	[52]
1,446	1,459	+13	CC and CCH in the rings	[53]
1,319	–	–	C–H	[54]
–	1,377	–	CH_3	[55]
1,263	–	–	C–O stretching vibrations	[56]
1,052	1,063	+11	C–O	[57]
835	–	–	Vibration bond of CH_2	[58]
–	722	–	CH_2	[59]
524	519	−5	Peak of alkyl halide	[47]

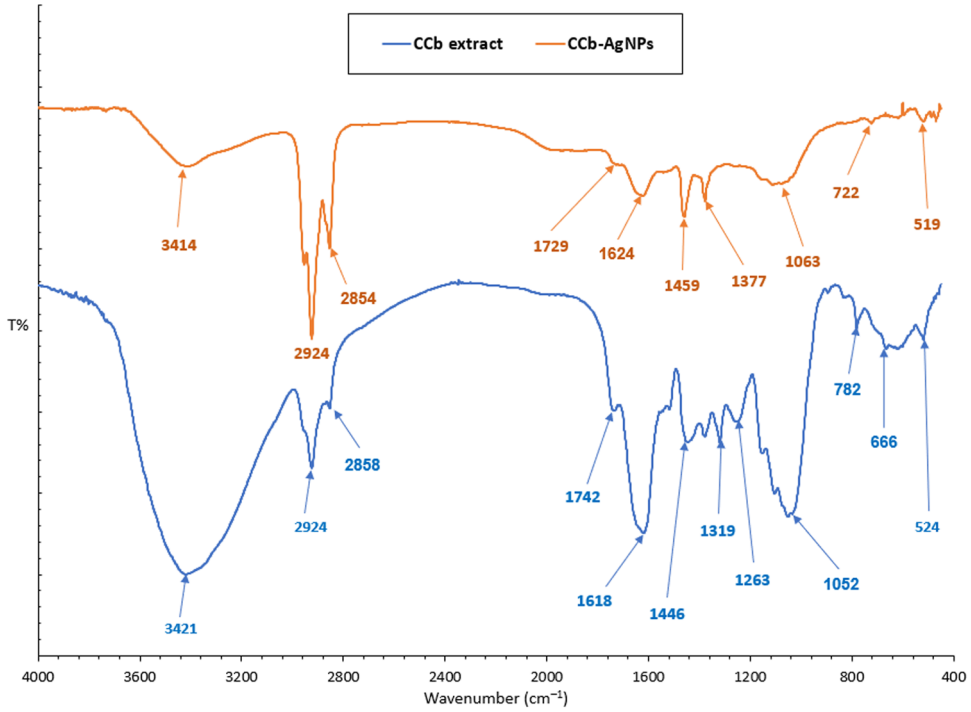

Figure 5: Comparative FT-IR spectra of the CCb extract and corresponding CCb-Ag-NPs.

used previously to assess the morphology, size, and distribution of nanoparticles [60]. SEM image also shows the rough contour of the biofabricated CCb-Ag-NPs, whose well-defined distribution agreed with Rasheed et al. [61].

3.3.3 Zeta potential of CCb-Ag-NPs

Zeta potential analysis was performed to measure the electrophoretic mobility of NPs and reflects the surface charge and stability of NPs [62]. Figure 7 shows the zeta potential of CCb-Ag-NPs at pH 5.6 and 25°C, where the mean value was −34.44 mV. CCb-Ag-NPs were stable due to the electrostatic repulsion [62], and a zeta potential of less than −15 mV ensures stability by creating a high-energy barrier [63]. These electrostatic repulsive forces, which are negatively charged, may also reduce the aggregation of MNPs [64]. CCb is also a reliable reducing and stabilizing agent. Abo-Elmagd et al. [65] attributed the high stability of NPs to bioorganic compounds that act as reducing and capping agents. Moreover, a Zeta sizer was used to measure the size of CCb-Ag-NPs as 40 nm.

3.3.4 EDS spectra of CCb-Ag-NPs

A large amount of silver (28.87%) was discernible at a wavelength of about 3 keV (Figure 8), confirming the presence of elementary silver at the nanoscale that could be attributed to its high SPR [66]. Due to SPR, Ag-NPs typically exhibit a prominent optical absorption peak at about 3 keV [62]. Other additional peaks were detected, such as C, O, Cl, and K, with mass% of 27.98, 36.83, 4.27, and 2.05, which indicated that biomolecules capped the biofabricated CCb-Ag-NPs.

3.3.5 XRD pattern of CCb-Ag-NPs

The XRD pattern of CCb-Ag-NPs is shown in Figure 9. It has been found from the XRD pattern that the maximum biofabricated phase is related to CCb-Ag-NPs, which denotes the formation of AgNPs in the sample. The diffraction lines positioned at 27°, 32°, 38°, 44°, 46°, 54°,57°, and 64° are related to the (110), (111), (200), (210), (211), (220), (220), and (310) (*hkl*) planes of metallic silver, respectively. According to many studies and the set (*hkl*) planes of the crystal, there is further indication that silver is crystallized. In Figure 9 and Table 2, red denotes Ag (87%) and blue denotes AgCl (13%), indicating the purity and stability of CCb-Ag-NPs. According to Hamouda et al. [67], the atomic spacing of protein-capped IEPS-Ag-NPs yields four noticeable peaks at 2θ values of 38.16°, 46.35°, 64.08°, and 77.71°, which matched the (111), (200), (220), and (311) (*hkl)* planes of the crystallographic structure (face-centered cubic). Ag-NPs biofabricated by *Ulva fasciata* generated

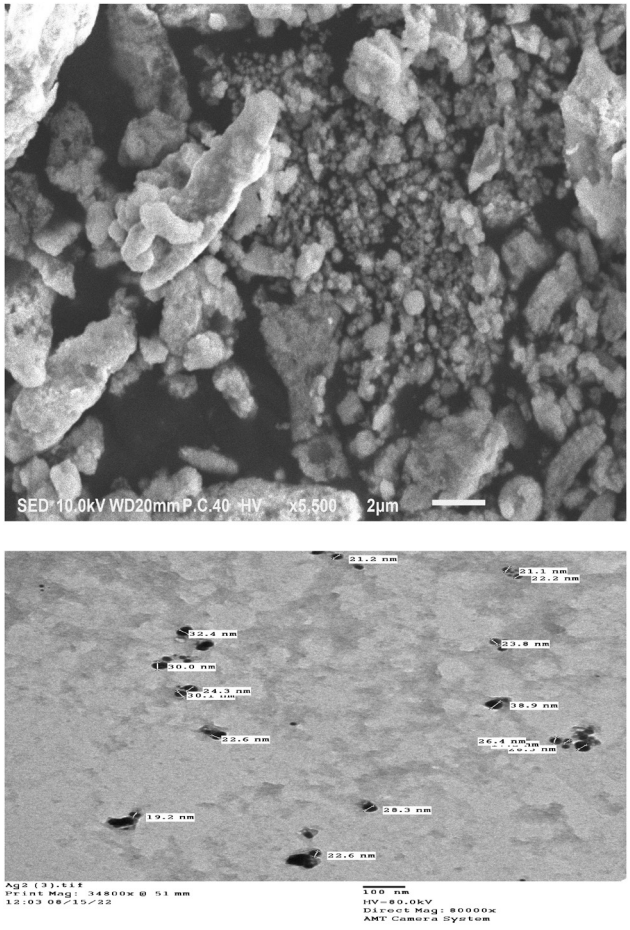

Figure 6: SEM and TEM image of biofabricated CCb-Ag-NPs.

five peaks at 2θ of 27°, 32°, 46°, 57°, and 76° corresponding to (111), (200), (220), (222), and (331) [68], whereas those biofabricated by *Turbinaria turbinata* showed visible peaks at 2θ 27.66°, 32°, 46°, 54°, 57°, 67°, 74°, and 76°, which matched the lattice planes (*hkl)* at (110), (111), (200), (220), (311), (222), (400), (331), and (420), confirming the crystallinity of Ag-NPs [69,70]. According to XRD, the average size ranged from 21.76 to 79.44. The major crystalline peak was investigated at 2θ (32.29°) with an intensity of 100% and a crystalline size of 37.12 nm. The size obtained by XRD was larger than that obtained by TEM and may be a personification step in the TEM procedure [71].

3.4 Biological activity

3.4.1 Antibacterial activity of CCb-Ag-NPs

Figure 10 shows the antimicrobial activity of pristine CCb-Ag-NPs, MEM/CCb-Ag-NPs, and FOX/CCb-Ag-NPs against three pathogenic bacterial strains. For *E. coli* (ATCC 25922), the inhibition zones of the freshly prepared CCb-Ag-NPs, FOX, FOX/CCb-Ag-NPs, MEM, and MEM/CCb-Ag-NPs were 7.6, 3.7, 10.3, 4.9, and 28.4 mm, respectively. For *E. coli* (ATCC 8739), the inhibition zones were 11.8, 9.6, 14.2, 18.6, and 23.3 mm for CCb-Ag-NPs, FOX, FOX/CCb-Ag-NPs, MEM, and MEM/CCb-Ag-NPs, respectively. For *P. aeruginosa* (ATCC 90274), the inhibition zones were 7.3, 6.8, 10.7, 16.6, and 22.1 for CCb-Ag-NPs, FOX, FOX/CCb-Ag-NPs, MEM, and MEM/CCb-Ag-NPs (Figure 11).

The prevalence of antibiotic-resistant *E. coli* and *P. aeruginosa* strains is a public health problem worldwide, and their eradication has become progressively difficult as a result of their notable capacity to resist already-used antibiotics [72,73]. Ag-NPs can help combat bacterial pathogens, as Ag^+ can bind to different bacterial cell components, such as the cell wall, and enable cytoplasm to flow from the injured cell wall [74]. Although the mechanisms behind the bactericidal activity of Ag-NPs or the released Ag^+ ion are poorly characterized, the synthesized Ag-NPs exert bactericidal activity against several bacterial species [75]. The synthesized NPs that are partially positive can adhere to the membrane of anionic bacterial cells through electrostatic interactions, which depolarize the membrane and perturb its permeability of internal cell contents like enzymes, proteins, DNA, and metabolic components leak, resulting in bacterial cell death [76]. Some reports [77,78] attributed the bactericidal potential of Ag-NPs to their smaller size, which interacts with the bacterial cell, damages respiratory enzymes, and reduces intracellular ATP levels, and other mechanisms include silver ion stress and the generation of reactive oxygen species. Other studies [79] claim that Ag-NPs coupled with antibiotics are more effective against Gram-negative bacteria than Gram-positive ones. Our data agree with Hamouda et al. [14], who studied the synergetic bactericidal effect of both synthesized Ag-NPs alone and cefaxone-conjugated NPs against *E. coli*.

3.4.2 Effect of fabricated CCb-Ag-NPs on wheat germination

The effects of the biofabricated CCb-Ag-NPs on the growth of *Triticum aestivum* seedlings were assessed based on the parameters of germination percentage, CL (mm), and RRL (mm) (Figure 12). Different concentrations (10, 20, 40, 80, and 160 mg·mL^{-1}) of CCb-Ag-NPs were used, and the results are shown in Figure 13(a)–(c). Low concentrations (10 and 20 mg·mL^{-1}) of CCb-Ag-NPs enhanced the *Triticum aestivum* germination percentage, CL, and RRL (Figure 13). However, higher concentrations (40, 80, and 160 mg·mL^{-1}) reduced these parameters.

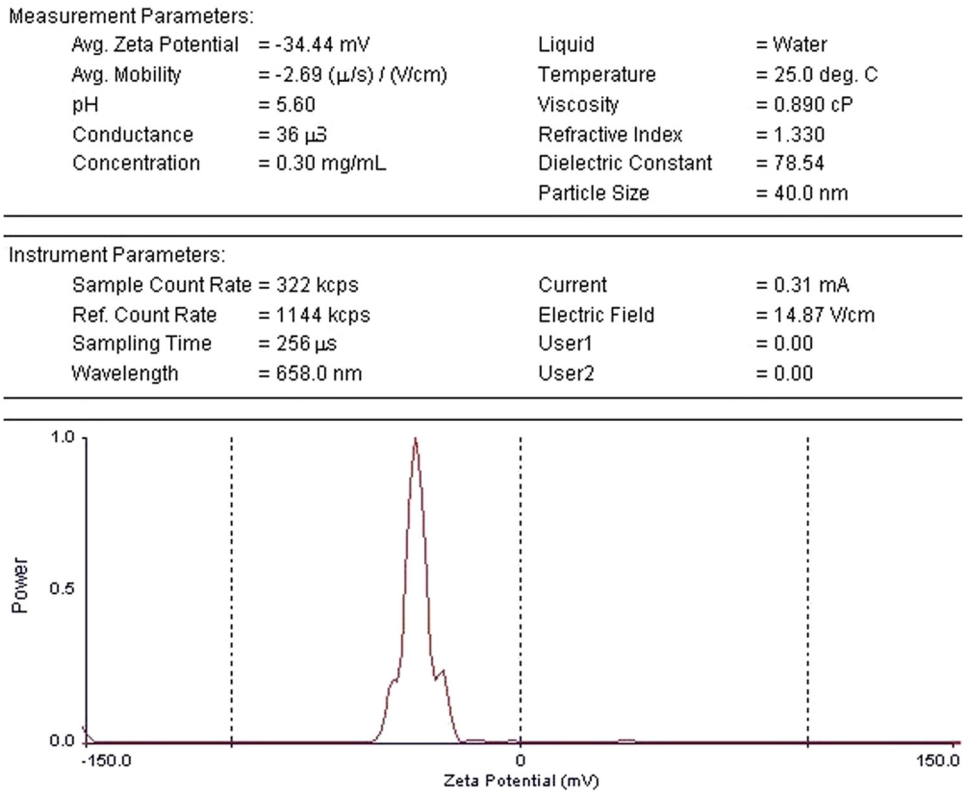

Figure 7: Zeta potential analysis of biofabricated CCb-Ag-NPs.

Both chemical and physical properties of the synthesized Ag-NPs, such as shape, size, concentration, and surface coatings, can detect inhibitory and stimulatory action, as well as other experimental parameters (dosage, exposure period, and plant species) that play a vital role in the germination and the subsequent growth process [36,80]. Soaking plant seeds using Ag-NPs can stimulate several chemical pathways, such as breaking of dormancy, growth inhibitory metabolite, hydrolysis or imbibition, and enzyme activation

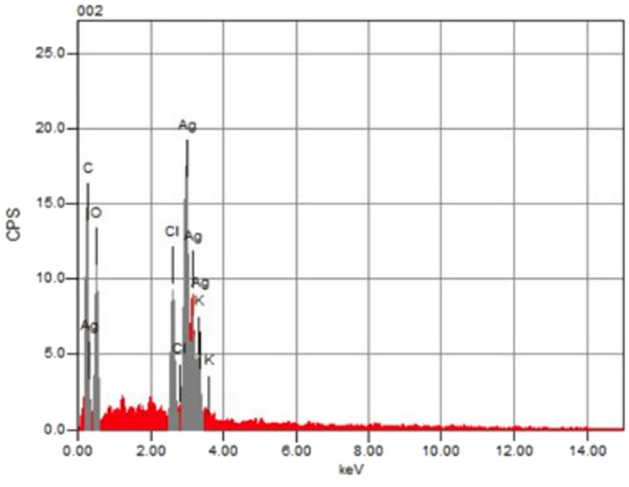

Formula	mass%	Atom%	Sigma	Net	K ratio	Line
C	27.98	45.93	0.08	6070	0.0023751	K
O	36.83	45.39	0.37	5358	0.0095811	K
Cl	4.27	2.37	0.07	6950	0.0047121	K
K	2.05	1.04	0.10	2816	0.0023246	K
Ag	28.87	5.28	0.32	27292	0.0265249	L
Total	100.00	100.00				

Figure 8: EDS spectrum of biofabricated CCb-Ag-NPs.

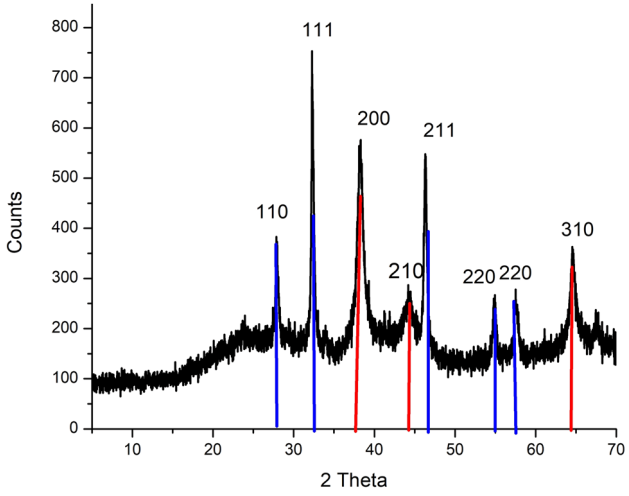

Figure 9: XRD patterns of the biofabricated CCb-Ag-NPs.

Table 2: XRD data for CCb-Ag-NPs

D (Å)	2*θ*	Intensity (%)	*D* (nm)	*hkl*
3.19707	27.884	45.0	27.11	110
2.76956	32.297	100	37.12	111
2.35742	38.144	77.5	79.44	200
2.04741	44.201	25.9	79.44	210
1.95968	46.292	73.1	34.84	211
1.67344	54.814	21.8	30.32	220
1.60211	57.476	19.0	79.44	220
1.44267	64.544	34.0	21.76	310

[36,81]. Previous studies [36] reported that low dosages of Ag-NPs (25–50 mg·mL^{-1}) stimulate wheat germination and other growth parameters. AgNPs are able to increase α-amylase activity causing higher soluble sugars that support seedlings in the early growth stage, and AgNPs were also found to have a stimulation effect on the aquaporin genes in germinating seeds [82]. Previous studies [36] hypothesized that AgNPs can enhance seed germination with at least three probable mechanisms, including (i) the formation of nanopores in the seed coat, (ii) a generation of reactive oxygen species, and (iii) a nanocatalyst for improving starch-degrading enzyme activity.

3.4.3 Effect of CCb-Ag-NPs on erythrocyte hemolysis

Figures 14 and 15 represent the hemolytic activity of CCb-Ag-NPs, where their activity increased with the dose of CCb-Ag-NPs. Erythrocyte hemolysis results from the direct interaction between Ag-NPs and RBCs as nanoparticles become more ionized and release Ag^{+} according to the particle surface area response [83]. The distinctive structures of Ag-NPs, such as their surface area and shape, interfere with the hemolytic activity of their RBCs. Hemolysis occurs when the membrane of the RBCs is compromised, resulting in hemoglobin leakage into surrounding plasma and health risks [84]. Indeed, Ag-NPs synthesized using plant extracts were found to have a low toxic effect

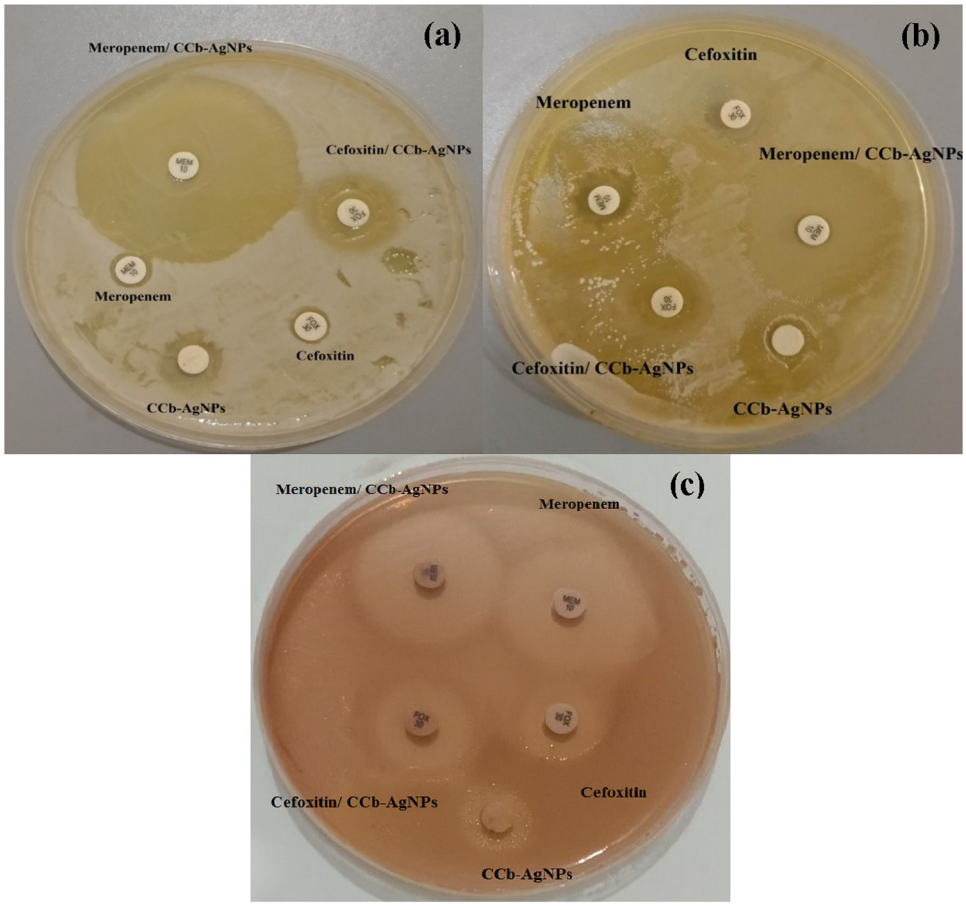

Figure 10: Antibacterial activity (zone of inhibition) of CCb-Ag-NPs against *E. coli* (ATCC 25922) (a), *E. coli* (ATCC 8739) (b), and *P. aeruginosa* (ATCC 90274) (c).

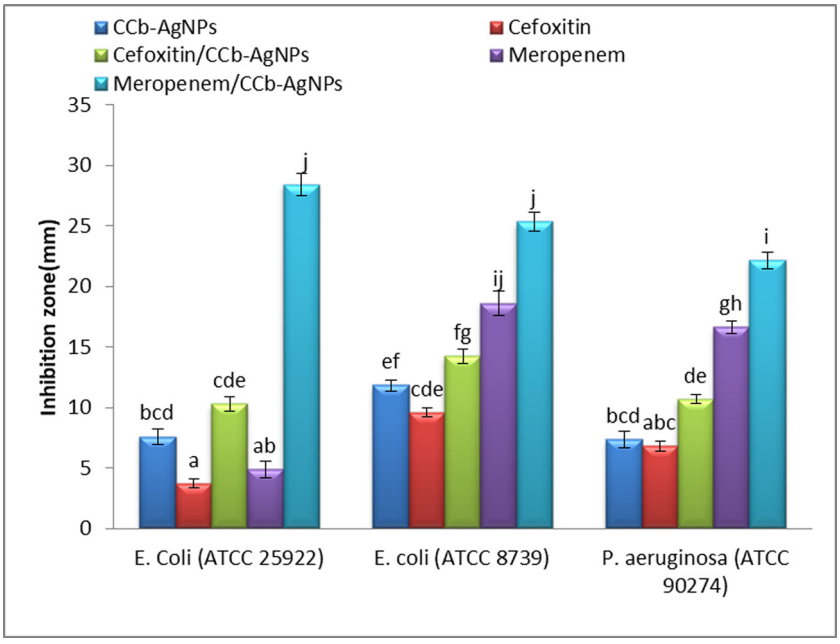

Figure 11: Antibacterial activity of CCb-Ag-NPs against *E. coli* (ATCC 25922), *E. coli* (ATCC 8739), and *P. aeruginosa* (ATCC 90274). Different letters have significant values.

Figure 12: Effect of different concentrations of CCb-Ag-NPs on *Triticum aestivum* seed germination.

against erythrocytes. The hemolytic activity of AgNPs was tested and formulated for biological activities, such as antibacterial activity, to estimate its biosafety and hemocompatibility as well as to detect bioactive components in the plant extracts and clarify the interaction mechanisms of the bioactive molecules with the precursor Ag salt [85].

4 Conclusions

Owing to their exceptional antibacterial properties, Ag-NPs have become one of the most promising materials for fighting drug-resistant bacteria. The synthesis, characterization, and use of nanostructured materials are then the

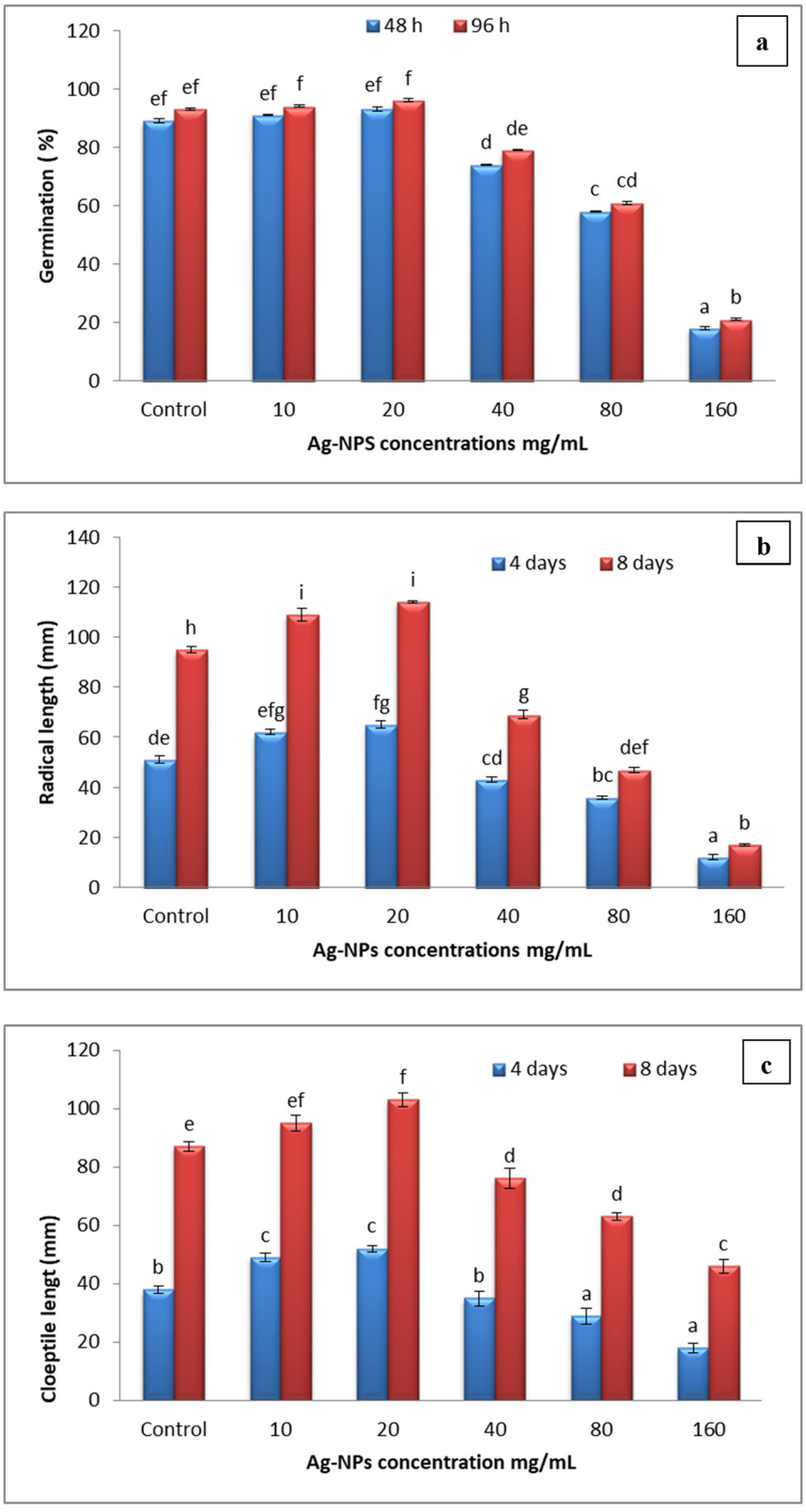

Figure 13: Effect of different concentrations (0, 10, 20, 40, 80, and 160 mg·mL^{-1}) of CCb-Ag-NPs on *Triticum aestivum* seed germination (a), CL (mm) (b), and RRL (mm) (c).

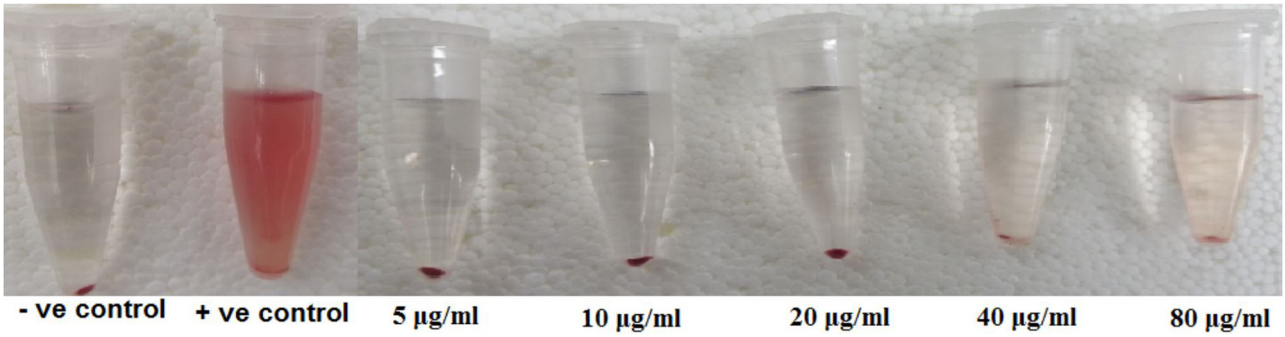

Figure 14: Hemolytic activity of different concentrations (5, 10, 20, 40, and 80 µg·mL^{-1}) of CCb-Ag-NPs.

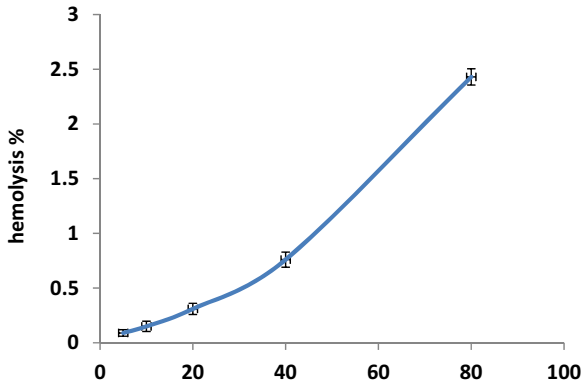

Figure 15: Percentage of hemolysis caused by CCb-Ag-NPs.

main goals of nanoscience and nanotechnology. In the current study, a simple, non-toxic, and reliable approach was used to fabricate Ag-NPs using the CCb aqueous extract (a popular name for *Uncaria tomentosa* L.). Different techniques have been used to characterize the fabricated CCb-Ag-NPs. The antibacterial activity, wheat seed germination, and hemolytic activity of the fabricated CCb-Ag-NPs were studied and evaluated. The findings are summarized as follows:

- The results of UV–Vis spectroscopy revealed that the optimal conditions for the biofabrication of CCb-Ag-NPs were the ratio between the CCb aqueous extract to 1 mM $AgNO_3$ solution (1:7), temperature (80°C), and pH (9.0).
- FT-IR gave a detailed picture of the various active groups in the CCb aqueous extract and the fabricated CCb-Ag-NPs, indicating that the presence of these active groups plays a role in reducing Ag ions and stabilizing CCb-Ag-NPs.
- SEM and TEM analysis results showed that the sizes of the CCb-Ag-NPs ranged from 19.2 to 38.5 nm, with a good distribution and no clusters.
- EDS and XRD results confirmed the presence of elementary silver (28.87%) and the formation of crystalline Ag-NPs.
- The stability of CCb-Ag-NPs was analyzed by zeta potential measurements. A negative zeta potential mean value of −34.44 mV proved the stability of the CCb-Ag-NPs.
- In conjunction with antibiotics, CCb-Ag-NPs exerted antibacterial activity against three MEM and FOX-resistant bacterial strains. The zone of inhibition is comparatively higher in the nanoparticle conjugate with antibiotics than in the individual performances. The biofabricated CCb-Ag-NPs have a synergistic bactericidal potential (accompanied by antibiotics) and advantages as biocontrol mediators for the studied pathogenic bacteria (*E. coli* and *P. aeruginosa*) due to their stability and small size.
- Low concentrations of biofabricated CCb-Ag-NPs enhanced the germination percentage, CL, and RRL of *Triticum aestivum* seeds, while high concentrations reduced these parameters. The results indicated that the chemical and physical characteristics of the biofabricated CCb-Ag-NPs, as well as other experimental parameters (dosage, exposure period, and plant species), play a vital role in the germination and the subsequent growth process.
- CCb-Ag-NPs showed hemolytic activity, and their activity increased with increasing doses of CCb-Ag-NPs. The unique surface area and morphology of CCb-AgNP interfere with the red blood cells' ability to hemolyze.
- The biofabricated CCb-AgNPs may have promising applications in the medicine, agriculture, and pharmaceutical industries.

Funding information: The authors state no funding involved.

Author contributions: Reem M. Alghanmi: conceptualization, methodology, and writing – original draft, visualization and supervision; Ragaa A. Hamouda: formal analysis, writing – original draft, visualization, and supervision; Aisha H. Al-Moubaraki: writing – review and editing;

Afnan A. Allouzi: investigation, resources, and writing – original draft; Muhammad A. Abuelmagd: investigation, resources, and writing – original draft.

Conflict of interest: The authors state no conflict of interest.

Data availability statement: The datasets generated during and/or analyzed during the current study are available from the corresponding author on reasonable request.

References

[1] Banin E, Hughes D. Bacterial pathogens, antibiotics and antibiotic resistance. FEMS Microbiol Rev. 2017;14:450–2.

[2] Wilczewska AZ, Niemirowicz K, Markiewicz KH, Car H. Nanoparticles as drug delivery systems. Pharmacol Rep. 2012;64:1020–37. doi: 10.1016/S1734-1140(12)70901-5.

[3] Ibraheem DR, Hussein NN, Sulaiman GM, Mohammed HA, Khan RA, Al Rugaie O. Ciprofloxacin-loaded silver nanoparticles as potent nano-antibiotics against resistant pathogenic bacteria. Nanomaterials. 2022;12:2808. doi: 10.3390/nano12162808.

[4] Varadavenkatesan T, Pai S, Vinayagam R, Selvaraj R. Characterization of silver nano-spheres synthesized using the extract of Arachis hypogaea nuts and their catalytic potential to degrade dyes. Mater Chem Phys. 2021;272:125017. doi: 10.1016/j.matchemphys.2021.125017.

[5] Hu D, Gao T, Kong X, Ma N, Fu J, Meng L, et al. Ginger (Zingiber officinale) extract mediated green synthesis of silver nanoparticles and evaluation of their antioxidant activity and potential catalytic reduction activities with Direct Blue 15 or Direct Orange 26. PLoS One. 2022;17:1–22. doi: 10.1371/journal.pone.0271408.

[6] Shet VB, Kumar PS, Vinayagam R, Selvaraj R, Vibha C, Rao S, et al. Cocoa pod shell mediated silver nanoparticles synthesis, characterization, and their application as nanocatalyst and antifungal agent. Appl Nanosci. 2023;13:4235–45. doi: 10.1007/s13204-023-02873-8.

[7] Deng H, McShan D, Zhang Y, Sinha SS, Arslan Z, Ray PC, et al. Mechanistic Study of the Synergistic Antibacterial Activity of Combined Silver Nanoparticles and Common Antibiotics. Environ Sci Technol. 2016;50:8840–8. doi: 10.1021/acs.est.6b00998.

[8] Haverkamp RG, Marshall AT. The mechanism of metal nanoparticle formation in plants: Limits on accumulation. J Nanopart Res. 2009;11:1453–63. doi: 10.1007/s11051-008-9533-6.

[9] Makarov VV, Makarova SS, Love AJ, Sinitsyna OV, Dudnik AO, Yaminsky IV, et al. Biosynthesis of stable iron oxide nanoparticles in aqueous extracts of hordeum vulgare and rumex acetosa plants. Langmuir. 2014;30:5982–8. doi: 10.1021/la5011924.

[10] Dauthal P, Mukhopadhyay M. Noble metal nanoparticles: Plant-mediated synthesis, mechanistic aspects of synthesis, and applications. Ind Eng Chem Res. 2016;55:9557–77. doi: 10.1021/acs.iecr.6b00861.

[11] Anees Ahmad S, Sachi Das S, Khatoon A, Tahir Ansari M, Afzal M, Saquib Hasnain M, et al. Bactericidal activity of silver nanoparticles: A mechanistic review. Mater Sci Energy Technol. 2020;3:756–69. doi: 10.1016/j.mset.2020.09.002.

[12] Ihtisham M, Noori A, Yadav S, Sarraf M, Kumari P, Brestic M, et al. Silver nanoparticle's toxicological effects and phytoremediation. Nanomaterials. 2021;11:1–18. doi: 10.3390/nano11092164.

[13] Ferdous Z, Nemmar A. Health impact of silver nanoparticles: A review of the biodistribution and toxicity following various routes of exposure. Int J Mol Sci. 2020;21:1–31. doi: 10.3390/ijms21072375.

[14] Hamouda RA, Hussein MH, Abo-elmagd RA, Bawazir SS. Synthesis and biological characterization of silver nanoparticles derived from the cyanobacterium Oscillatoria limnetica. Sci Rep. 2019;9:1–17. doi: 10.1038/s41598-019-49444-y.

[15] Bhole R, Gonsalves D, Murugesan G, Narasimhan MK, Srinivasan NR, Dave N, et al. Superparamagnetic spherical magnetite nanoparticles: Synthesis, characterization and catalytic potential. Appl Nanosci. 2023;13:6003–14. doi: 10.1007/s13204-022-02532-4.

[16] El Shafey AM. Green synthesis of metal and metal oxide nanoparticles from plant leaf extracts and their applications: A review. Green Process Synth. 2020;9:304–39. doi: 10.1515/gps-2020-0031.

[17] Baeshen NA, Almulaiky YQ, Afifi M, Al-Farga A, Ali HA, Baeshen NN, et al. GC-MS analysis of bioactive compounds extracted from plant rhazya stricta using various solvents. Plants. 2023;12:1–13. doi: 10.3390/plants12040960.

[18] Roy A, Ananda Murthy HC, Ahmed HM, Islam MN, Prasad R. Phytogenic synthesis of metal/metal oxide nanoparticles for degradation of dyes. J Renew Mater. 2022;10:1911–30. doi: 10.32604/jrm.2022.019410.

[19] Choudhary MK, Kataria J, Sharma S. Evaluation of the kinetic and catalytic properties of biogenically synthesized silver nanoparticles. J Clean Prod. 2018;198:882–90. doi: 10.1016/j.jclepro.2018.09.015.

[20] Ajlouni AW, Hamdan EH, Alshalawi RAE, Shaik MR, Khan M, Kuniyil M, et al. Green synthesis of silver nanoparticles using aerial part extract of the Anthemis pseudocotula boiss. plant and their biological activity. Molecules. 2023;28:246. doi: 10.3390/molecules28010246.

[21] Khan AN, Ali Aldowairy NN, Saad Alorfi HS, Aslam M, Bawazir WAB, Hameed A, et al. Excellent antimicrobial, antioxidant, and catalytic activities of medicinal plant aqueous leaf extract derived silver nanoparticles. Processes. 2022;10:1949. doi: 10.3390/pr10101949.

[22] Ajay S, Panicker JS, Manjumol KA, Subramanian PP. Photocatalytic activity of biogenic silver nanoparticles synthesized using Coleus Vettiveroids. Inorg Chem Commun. 2022;144:109926.

[23] David L, Moldovan B. Green synthesis of biogenic silver nanoparticles for efficient catalytic removal of harmful organic dyes. Nanomaterials. 2020;10:202. doi: 10.3390/nano10020202.

[24] Riaz M, Suleman A, Ahmad P, Khandaker MU, Alqahtani A, Bradley DA, et al. Biogenic synthesis of AgNPs using aqueous bark extract of aesculus indica for antioxidant and antimicrobial applications. Crystals. 2022;12:252. doi: 10.3390/cryst12020252.

[25] Nayak D, Ashe S, Rauta PR, Kumari M, Nayak B. Bark extract mediated green synthesis of silver nanoparticles: Evaluation of antimicrobial activity and antiproliferative response against osteosarcoma. Mater Sci Eng C. 2016;58:44–52. doi: 10.1016/j.msec.2015.08.022.

[26] Joe MH, Jeong HT, Lee HM, Park HJ, Kim DH, Park DH, et al. Phytosynthesis of silver and gold nanoparticles using the hot water extract of mixed woodchip powder and their antibacterial efficacy. J Nanomater. 2017;2017:1–19. doi: 10.1155/2017/8734758.

[27] Abd El-Aziz ARM, Gurusamy A, Alothman MR, Shehata SM, Hisham SM, Alobathani AA. Silver nanoparticles biosynthesis using Saussurea costus root aqueous extract and catalytic degradation efficacy of safranin dye. Saudi J Biol Sci. 2021;28:1093–9. doi: 10.1016/j.sjbs.2020.11.036.
[28] Kumar B. Green synthesis of gold, silver, and iron nanoparticles for the degradation of organic pollutants in wastewater. J Compos Sci. 2021;5:219. doi: 10.3390/jcs5080219.
[29] Bao Y, He J, Song K, Guo J, Zhou X, Liu S. Plant-extract-mediated synthesis of metal nanoparticles. J Chem. 2021;2021:1–14. doi: 10.1155/2021/6562687.
[30] Reinhard KH. Uncaria tomentosa (Willd.) D.C.: Cat's claw, una de gato, or saventaro. J Altern Complement Med. 1999;5:143–51. doi: 10.1089/acm.1999.5.143.
[31] Elgegren M, Donayre A, Kim S, Galarreta BC, Nakamatsu J. Tridimensional Alginate Films with Cat's Claw (Uncaria tomentosa) Extract or Aloe Vera (Aloe barbadensis) Gel for Potential Use as Wound Dressings. Proceedings. 2021;69:1–8. doi: 10.3390/cgpm2020-07225.
[32] Shen J, Shalom J, Cock IE. The Antiproliferative Properties of Uncaria tomentosa Willd. DC. extracts against Caco2 and HeLa Cancer Cell Lines. Pharmacogn Commun. 2018;8:8–14. doi: 10.5530/pc.2018.1.3.
[33] Zargar M, Hamid AA, Bakar FA, Shamsudin MN, Shameli K, Jahanshiri F, et al. Green synthesis and antibacterial effect of silver nanoparticles using Vitex negundo L. Molecules. 2011;16:6667–76. doi: 10.3390/molecules16086667.
[34] Wikler MA. Methods for dilution antimicrobial susceptibility tests for bacteria that grow aerobically. Approved standard. Clsi. 2006;26:M7–A7.
[35] Li R, He J, Xie H, Wang W, Bose SK, Sun Y, et al. Effects of chitosan nanoparticles on seed germination and seedling growth of wheat (Triticum aestivum L.). Int J Biol Macromol. 2019;126:91–100. doi: 10.1016/j.ijbiomac.2018.12.118.
[36] Singh Y, Kaushal S, Sodhi RS. Biogenic synthesis of silver nanoparticles using cyanobacterium: Leptolyngbya sp. WUC 59 cell-free extract and their effects on bacterial growth and seed germination. Nanoscale Adv. 2020;2:3972–82. doi: 10.1039/d0na00357c.
[37] Mulvaney P. Surface plasmon spectroscopy of nanosized metal particles. Langmuir. 1996;12:788–800. doi: 10.1021/la9502711.
[38] Prakash P, Gnanaprakasam P, Emmanuel R, Arokiyaraj S, Saravanan M. Green synthesis of silver nanoparticles from leaf extract of Mimusops elengi, Linn. for enhanced antibacterial activity against multi drug resistant clinical isolates. Colloids Surf B Biointerfaces. 2013;108:255–9. doi: 10.1016/j.colsurfb.2013.03.017.
[39] Abo-Elmagd RA, Hamouda RA, Hussein MH. Phycotoxicity and catalytic reduction activity of green synthesized Oscillatoria gelatin-capped silver nanoparticles. Sci Rep. 2022;12:20378. doi: 10.1038/s41598-022-22976-6.
[40] Lowry OH, Rosebrough NJ, Farr AL, Randall RJ. Protein measurement with the Folin phenol reagent. J Biol Chem. 1951;193:265–75. doi: 10.1016/s0021-9258(19)52451-6.
[41] Govindaraju K, Kiruthiga V, Kumar VG, Singaravelu G. Extracellular synthesis of silver nanoparticles by a marine alga, Sargassum wightii grevilli and their Antibacterial effects. J Nanosci Nanotechnol. 2009;9:5497–501. doi: 10.1166/jnn.2009.1199.
[42] Jena J, Pradhan N, Prasad Dash B, Behari Sukla L. kumar Panda Affiliations P. Biosynthesis and characterization of silver nanoparticles using microalga Chlorococcum humicola and its antibacterial activity. Int J Nanomater Biostruct. 2013;3:1–8.
[43] Ider M, Abderrafi K, Eddahbi A, Ouaskit S, Kassiba A. Silver metallic nanoparticles with surface plasmon resonance: synthesis and characterizations. J Clust Sci. 2017;28:1051–69. doi: 10.1007/s10876-016-1080-1.
[44] Ahmad N, Fozia, Jabeen M, Haq ZU, Ahmad I, Wahab A, et al. Green fabrication of silver nanoparticles using euphorbia serpens kunth aqueous extract, their characterization, and investigation of its in vitro antioxidative, antimicrobial, insecticidal, and cytotoxic activities. Biomed Res Int. 2022;2022:1–11. doi: 10.1155/2022/5562849.
[45] Veerasamy R, Xin TZ, Gunasagaran S, Xiang TFW, Yang EFC, Jeyakumar N, et al. Biosynthesis of silver nanoparticles using mangosteen leaf extract and evaluation of their antimicrobial activities. J Saudi Chem Soc. 2011;15:113–20.
[46] Andreescu D, Eastman C, Balantrapu K, Goia DV. A simple route for manufacturing highly dispersed silver nanoparticles. J Mater Res. 2007;22:2488–96. doi: 10.1557/jmr.2007.0308.
[47] Jaast S, Grewal A. Green synthesis of silver nanoparticles, characterization and evaluation of their photocatalytic dye degradation activity. Curr Res Green Sustain Chem. 2021;4:100195. doi: 10.1016/j.crgsc.2021.100195.
[48] Rubio F, Gonçalves AC, Meneghel AP, Teixeira Tarley CR, Schwantes D, Coelho GF. Removal of cadmium from water using by-product Crambe abyssinica Hochst seeds as biosorbent material. Water Sci Technol. 2013;68:227–33. doi: 10.2166/wst.2013.233.
[49] Portaccio M, Errico S, Chioccarelli T, Cobellis G, Lepore M. Fourier-Transform Infrared Microspectroscopy (FT-IR) study on caput and cauda mouse spermatozoa. Multidiscip Digit Publ Inst Proc. 2019;42:19. doi: 10.3390/ecsa-6-06537.
[50] Sukprasert J, Thumanu K, Phung-On I, Jirarungsatean C, Erickson LE, Tuitemwong P, et al. Synchrotron FTIR light reveals signal changes of biofunctionalized magnetic nanoparticle attachment on salmonella sp. J Nanomater. 2020;2020:1–12. doi: 10.1155/2020/6149713.
[51] Kemel K, Baillet-Guffroy A, Faivre V, Laugel C. ATR-FTIR characterization of janus nanoparticles—Part II: follow-up skin application. J Pharm Sci. 2019;108:3366–71. doi: 10.1016/j.xphs.2019.06.018.
[52] Topală CM, Tătaru LD, Ducu C. ATR-FTIR spectra fingerprinting of medicinal herbs extracts prepared using microwave extraction. Arab J Med Aromat. Plants. 2017;3:1–9.
[53] Ullah R, Ahmad I, Zheng Y. Fourier Transform infrared Spectrosc "bisphenol A". J Spectrosc. 2016;2016:1–5.
[54] Kwon SM, Jang JH, Lee SH, Park SB, Kim NH. Change of heating value, pH and FT-IR spectra of charcoal at different carbonization temperatures. J Korean Wood Sci Technol. 2013;41:440–6. doi: 10.5658/WOOD.2013.41.5.440.
[55] Pennington BD, Ryntz RA, Urban MW. Stratification in thermoplastic olefins (TPO); Photoacoustic FT-IR depth profiling studies. Polymer (Guildf). 1999;40:4795–803. doi: 10.1016/S0032-3861(98)00714-9.
[56] Altameme HJ, Hameed IH, Abu-Serag NA. Analysis of bioactive phytochemical compounds of two medicinal plants, equisetum arvense and alchemila valgaris seeds using gas chromatography-mass spectrometry and fourier-transform infrared spectroscopy. Malays Appl Biol. 2015;44:47–58.
[57] Cintrón MS, Hinchliffe DJ. FT-IR examination of the development of secondary cell wall in cotton fibers. Fibers. 2015;3:30–40. doi: 10.3390/fib3010030.
[58] Ahmed H. Spectroscopic characterization of leukemia samples using laser raman and fourier transform infrared spectroscopy.

Doctoral dissertation. Sudan Univesity of Science and Technology; 2011.
[59] Poiana MA, Alexa E, Munteanu MF, Gligor R, Moigradean D, Mateescu C. Use of ATR-FTIR spectroscopy to detect the changes in extra virgin olive oil by adulteration with soybean oil and high temperature heat treatment. Open Chem. 2015;13:689–98. doi: 10.1515/chem-2015-0110.
[60] Khatami M, Sharifi I, Nobre MAL, Zafarnia N, Aflatoonian MR. Waste-grass-mediated green synthesis of silver nanoparticles and evaluation of their anticancer, antifungal and antibacterial activity. Green Chem Lett Rev. 2018;11:125–34. doi: 10.1080/17518253.2018.1444797.
[61] Rasheed T, Bilal M, Li C, Nabeel F, Khalid M, Iqbal HMN. Catalytic potential of bio-synthesized silver nanoparticles using Convolvulus arvensis extract for the degradation of environmental pollutants. J Photochem Photobiol B Biol. 2018;181:44–52. doi: 10.1016/j.jphotobiol.2018.02.024.
[62] Baharara J, Namvar F, Ramezani T, Hosseini N, Mohamad R. Green synthesis of silver nanoparticles using achillea biebersteinii flower extract and its anti-angiogenic properties in the rat aortic ring model. Molecules. 2014;19:4624–34. doi: 10.3390/molecules19044624.
[63] Sankar R, Karthik A, Prabu A, Karthik S, Shivashangari KS, Ravikumar V. Origanum vulgare mediated biosynthesis of silver nanoparticles for its antibacterial and anticancer activity. Colloids Surf B Biointerfaces. 2013;108:80–4. doi: 10.1016/j.colsurfb.2013.02.033.
[64] Suriyakalaa U, Antony JJ, Suganya S, Siva D, Sukirtha R, Kamalakkannan S, et al. Hepatocurative activity of biosynthesized silver nanoparticles fabricated using Andrographis paniculata. Colloids Surf B Biointerfaces. 2013;102:189–94. doi: 10.1016/j.colsurfb.2012.06.039.
[65] Abo-Elmagd RA, Hussein MH, Hamouda RA, Shalan AE, Abdelrazak A. Statistical optimization of photo-induced biofabrication of silver nanoparticles using the cell extract of: Oscillatoria limnetica: insight on characterization and antioxidant potentiality. RSC Adv. 2020;10:44232–46. doi: 10.1039/d0ra08206f.
[66] Jain N, Bhargava A, Rathi M, Dilip RV, Panwar J. Removal of protein capping enhances the antibacterial efficiency of biosynthesized silver nanoparticles. PLoS One. 2015;10:0134337. doi: 10.1371/journal.pone.0134337.
[67] Hamouda RA, Hussein MH, Elhadary AMA, Abuelmagd MA. Extruded polysaccharide/protein matrix from Arthrospira platensis cultures mediated silver nanoparticles biosynthesis and capping. Appl Nanosci. 2020;10:3839–55. doi: 10.1007/s13204-020-01490-z.
[68] Hamouda RA, Yousuf WE, Abdeen EE, Mohamed A. Biological and Chemical Synthesis of Silver Nanoparticles: Characterization, MIC and Antibacterial Activity against Pathogenic Bacteria. J Chem Pharm Res. 2019;11:1–12.
[69] Abdellatif KF, Hamouda RA, El-Ansary MSM. Green nanoparticles engineering on root-knot nematode infecting eggplants and their effect on plant dna modification. Iran J Biotechnol. 2016;14:250–9. doi: 10.15171/ijb.1309.
[70] El Bialy BE, Hamouda RA, Khalifa KS, Hamza HA. Cytotoxic effect of biosynthesized silver nanoparticles on Ehrlich ascites tumor cells in mice. Int J Pharmacol. 2017;13:134–44.
[71] Hamouda RA, Abd El-Mongy M, Eid KF. Comparative study between two red algae for biosynthesis silver nanoparticles capping by SDS: Insights of characterization and antibacterial activity. Microb Pathog. 2019;129:224–32. doi: 10.3390/molecules27051602.
[72] Pang Z, Raudonis R, Glick BR, Lin TJ, Cheng Z. Antibiotic resistance in Pseudomonas aeruginosa: mechanisms and alternative therapeutic strategies. Biotechnol Adv. 2019;37:177–92. doi: 10.1016/j.biotechadv.2018.11.013.
[73] Pormohammad A, Nasiri MJ, Azimi T. Prevalence of antibiotic resistance in escherichia coli strains simultaneously isolated from humans, animals, food, and the environment: A systematic review and meta-analysis. Infect Drug Resist. 2019;12:1181–97. doi: 10.2147/IDR.S201324.
[74] Sondi I, Salopek-Sondi B. Silver nanoparticles as antimicrobial agent: A case study on E. coli as a model for Gram-negative bacteria. J Colloid Interface Sci. 2004;275:177–82. doi: 10.1016/j.jcis.2004.02.012.
[75] Ipe DS, Kumar PTS, Love RM, Hamlet SM. Silver nanoparticles at biocompatible dosage synergistically increases bacterial susceptibility to antibiotics. Front Microbiol. 2020;11:1–11. doi: 10.3389/fmicb.2020.01074.
[76] Ali MA, Ahmed T, Wu W, Hossain A, Hafeez R, Masum MMI, et al. Advancements in plant and microbe-based synthesis of metallic nanoparticles and their antimicrobial activity against plant pathogens. Nanomaterials. 2020;10:1–24. doi: 10.3390/nano10061146.
[77] Das CGA, Kumar VG, Dhas TS, Karthick V, Govindaraju K, Joselin JM, et al. Antibacterial activity of silver nanoparticles (biosynthesis): A short review on recent advances. Biocatal Agric Biotechnol. 2020;27:101593. doi: 10.1016/j.bcab.2020.101593.
[78] Vanlalveni C, Lallianrawna S, Biswas A, Selvaraj M, Changmai B, Rokhum SL. Correction: green synthesis of silver nanoparticles using plant extracts and their antimicrobial activities: A review of recent literature. RSC Adv. 2022;12:16093.
[79] Perveen S, Safdar N, Chaudhry GeS, Yasmin A. Antibacterial evaluation of silver nanoparticles synthesized from lychee peel: individual versus antibiotic conjugated effects. World J Microbiol Biotechnol. 2018;34:1–12. doi: 10.1007/s11274-018-2500-1.
[80] Cvjetko P, Milošić A, Domijan AM, Vinković Vrček I, Tolić S, Peharec Štefanić P, et al. Toxicity of silver ions and differently coated silver nanoparticles in Allium cepa roots. Ecotoxicol Environ Saf. 2017;137:18–28. doi: 10.1016/j.ecoenv.2016.11.009.
[81] Yan A, Chen Z. Impacts of silver nanoparticles on plants: A focus on the phytotoxicity and underlying mechanism. Int J Mol Sci. 2019;20:1–21. doi: 10.3390/ijms20051003.
[82] Smirnov O, Kalynovskyi V, Yumyna Y, Zelena P, Levenets T, Kovalenko M, et al. Potency of phytosynthesized silver nanoparticles from Lathraea squamaria as anticandidal agent and wheat seeds germination enhancer. Biologia (Bratisl). 2022;77:2715–24. doi: 10.1007/s11756-022-01117-4.
[83] Lansdown ABG. A pharmacological and toxicological profile of silver as an antimicrobial agent in medical devices. Adv Pharmacol Sci. 2010;2010:1–16. doi: 10.1155/2010/910686.
[84] Choi J, Reipa V, Hitchins VM, Goering PL, Malinauskas RA. Physicochemical characterization and in vitro hemolysis evaluation of silver nanoparticles. Toxicol Sci. 2011;123:133–43. doi: 10.1093/toxsci/kfr149.
[85] Liaqat N, Jahan N, Khalil-ur-Rahman, Anwar T, Qureshi H. Green synthesized silver nanoparticles: Optimization, characterization, antimicrobial activity, and cytotoxicity study by hemolysis assay. Front Chem. 2022;10:952006. doi: 10.3389/fchem.2022.952006.